Desalination and Water Treatment
www.deswater.com

doi: 10.5004/dwt.2020.25759

191 (2020) 350–361
July

Optimization of microwave-enhanced oxidation of landfill leachate by response surface methodology

Chih-Jung Yeh[a], Shang-Lien Lo[a,*], Jeff Kuo[b], Yu-Chieh Chou[a]

[a]*Graduate Institute of Environmental Engineering, National Taiwan University, No. 1, Sec. 4, Roosevelt Rd., Taipei 106, Taiwan, R.O.C, Tel. +886 2 23625373; Fax: +886 2 23928821; email: sllo@ntu.edu.tw (S.-L. Lo), Tel. +886 2 33664394; Fax: +886 2 23928830; emails: s8825032@yahoo.com.tw (C.-J. Yeh), ycchou823@gmail.com (Y.-C. Chou)*
[b]*Department of Civil and Environmental Engineering, California State University Fullerton, CA 92834, USA, email: jkuo@Exchange.fullerton.edu (J. Kuo)*

Received 13 September 2019; Accepted 28 February 2020

ABSTRACT

Raw landfill leachate was treated using an enhanced microwave oxidation process for removals of total organic carbon (TOC), color, and organic compounds with double bonds (UV_{254}). Experimental factors, microwave (MW) power setting, reaction time, and initial persulfate (PS) concentration, were optimized via response surface methodology (RSM) with a Box–Behnken design. The analysis of variance was used to derive the prediction correlation coefficient and the relationship of each factor on the test parameters. The contour-line plots and surface plots revealed the optimal operating conditions for removals of three parameters. The initial PS concentration had the most significant effect on the removals of all three parameters. The highest removals of 79.5%, 100%, and 68.4% for TOC, color, and UV_{254} attained under separate optimal operating conditions, respectively. The optimal operating conditions for TOC, color, and UV_{254} removals as a whole were derived to be 447.7 W, 20.0 mM, and 116.3 min with removals of 78.8%, 100%, and 66.4%, respectively.

Keywords: Leachate degradation; Microwave; Chemical oxidation; Response surface methodology; Box–Behnken design

1. Introduction

Leachate is being produced from waste degradation and surface water infiltration in a typical landfill. Landfill leachate typically has elevated concentrations of compounds of concern, and its characteristics are changing with time [1]. It would have adverse impacts on the environment and human health without proper collection and treatment. Various leachate treatment methods have been developed and applied, including biological [2,3], physical-chemical [4,5], membrane [6,7], and advanced oxidation processes (AOPs) [8,9].

Microwave (MW) heating involves electromagnetic waves radiation and heat transfer. Under MW irradiation, dipolar molecules such as water will absorb MW energy, oscillate back and forth, and then convert the absorbed MW energy into thermal energy [10,11]. The principle of MW heating differs from traditional heating, and the heat conduction is from inside out [12]. Therefore, MW heating can increase the reaction rate to reduce the required treatment time. MW treatment technologies are being widely used in lignocellulosic biomass pyrolysis [13], direct dyes [14], and 4-nitrophenol degradation [15], to name a few.

Persulfate ($S_2O_8^{2-}$, PS) is a strong oxidizing agent, with a high oxidation-reduction potential (ORP) of 2.01 V [16], but it is quite stable under ambient conditions. It has been applied to the degradation of perfluorooctanoic acid (PFOA) [17], sulfadiazine (Sdz) [18], and polychlorinated biphenyls (PCBs) [19,20]. PS generates sulfate free radicals ($SO_4^{-\bullet}$)

* Corresponding author.

through activation processes (e.g., heat in Eq. (1)), and then reacted with organic matters [17,19].

$$S_2O_8^{2-} \xrightarrow{\text{heat}} SO_4^{-\bullet} + SO_4^{-\bullet}\left(\text{or } SO_4^{2-}\right) \quad (1)$$

Sulfate radical ($SO_4^{-\bullet}$) has a redox potential of 2.43 V [21], close to that of hydroxyl radical ($HO^{\bullet}$), 2.8 V [22]. Sulfate radical is more stable than hydroxyl radical (with a longer half-life) so that it has a better opportunity to react with organic matters when present [23].

Response surface methodology (RSM) is a statistical and optimization method for experimental design to obtain experimental data efficiently. It contains a two-dimensional (2D) graph and a three-dimensional (3D) graph. The former provides a 2D view where all points that have the same response are connected to produce contour-lines of constant responses. The latter displays the 3D view relationship in two dimensions with the factors on the *x*- and *y*-scales, while the response (*z*-scale) variable represented by a smooth surface. The 3D graph would be generated by calculating fitted removal responses (*z*-values) using the *x*- and *y*-variables while holding any additional factors constant at the values specified in the setting conditions [24]. Briefly, RSM can display the surface curvature changes in the response between two factors. It can tell whether the experiment of range understudy has a curvature. When the experimental region is near the optimal reaction conditions, the curvature of the real reaction surface increases. A multivariate quadratic regression equation (quadratic model) is used to fit the relationship between the experimental factors and the response values, and then to find the optimal operating conditions through regression analysis. Using RSM has many advantages, including a smaller number of experiments, less experimental costs, and more efficient experiments. In a multiple-factor experimental design, single or multiple response values of design optimization, as well as co-optimization, are the mainstreams of the RSM study. In recent years, the RSM has been widely used in biosorption technology [25], amoxicillin removal [26], and low-density polyethylene pyrolysis [27], to name a few.

The main RSM design approaches are Box–Behnken design (BBD) and central composite design (CCD). The former often used in the design of experiments with more than three factors and the levels setting values of these factors must be continuous. The design should generate sufficient data to fit a quadratic model; in other words, containing single, squared, and cross-product terms of three or more factors. The three experimental factors are considered as the graph variables for three axes (*X*, *Y*, and *Z*) with a center point of (0,0,0) and edge center points ($X \pm 1$, $Y \pm 1$, $Z \pm 1$) to constitute a cube and a sphere inside with a radius of $\sqrt{2}$ [28]. Therefore, the sphere should be rotatable (or nearly rotatable) and require 3 levels of each factor. In other words, all the experimental points are located on the equidistant endpoints without containing the level of the variables generated by the cube vertex (corner point) in the experiment. Each design can be thought of as a combination of a two-level (full or fractional) factorial design with an incomplete block. In each block, a certain number of factors are put through all combinations for the factorial design, while the remaining factors are kept at the central values. In short, a BBD design has treatment combinations for the RSM that are at the midpoints of the edges of the experimental space and at the center. Because the BBD does not contain corner points (the design points are all inside the sphere), it is thus assured that all design points are within the safe operating area.

Our research team has previously conducted several landfill leachate treatment studies using MW technology [29–31]. However, the RSM was not used in those studies to optimize the operating parameters. Optimization of such parameters is main desirable so that the treatment time, chemical usage, and cost can be reduced. The overall objective study was to use the RSM to optimize three factors (MW power setting, irradiation time, and initial PS concentration) for removals of three parameters (total organic carbon (TOC), color, and organic compounds containing double bonds (UV_{254})) from landfill leachates. In a graphical analysis, using the software would generate either a contour plot for a single pair of variables or separate contour plots for all possible pairs of variables. In this paper, only the core component of BBD experimental design in informative response surfaces are presented to save space. There will show the surface curvature changes in removals of these three parameters.

2. Experimental approaches

2.1. Materials and methods

Leachate samples used in this study were taken from the Sanjuku Sanitary Landfill, located in Taipei, Taiwan. This site occupies an area of about 65 ha. It started its operation in 1994 and closed in 2010. The leachate samples were collected in 25 L plastic containers and stored at 4°C before being used in the experiments. Table 1 summarizes the characteristics of the raw landfill leachate from August 2013 to August 2014. As shown, the BOD_5/COD ratios were relatively low and constant at 0.126–0.127, implying that the organic matters present in the leachate are not readily biodegradable [32]. When a specific UV absorbance (SUVA) value is greater than 4, leachate has more humic (larger organic molecules) fraction, while when smaller than 2, non-humic (smaller organic molecules) substances dominate. SUVA values of the raw leachate samples were 3.07–3.38, in the range between 2 and 4, implying that the contained organics were a mixture of humic and non-humic substances [33]. The averaged concentrations of TOC, color, and UV_{254} were 56.5 mg/L, 121 Pt-Co color units, and 1.648 cm^{-1}, respectively.

In our previous studies, each experiment used 50 mL of leachate (pre-filtered) with a specific initial PS ($S_2O_8^{2-}$) concentration of 4, 10, or 20 mM. The MW irradiation was provided by a Milestone Ethos plus MW system (Milestone Inc., USA). The MW power setting was 325, 550, or 775 W at 85°C, the irradiation time was 40, 70, or 130 min, which included preheating at the reaction temperature for 10 min [29–31].

For leachate analysis, TOC concentrations were determined following the W532.52C method (National Institute of Environmental Analysis, NIEA) by using an Aurora 1030 TOC analyzer (OI Analytical Co., USA). Color and UV_{254} measurements followed the NIEA W223.52B method, using a Helios Beta UV–Vis spectrophotometer (Thermo Fisher

Table 1
Characteristics of raw landfill leachate

Parameters	Values	Units
COD	137–233	mg/L
BOD_5	17.3–29.7	mg/L
BOD_5/COD ratio	0.126–0.127	
TOC	48.8–56.5	mg/L
pH	7.2–7.4	
Color	87–121	Pt-Co color units
UV_{254}	1.648–1.735	cm^{-1}
SUVA (UV_{254}/TOC × 100)	3.07–3.38	L/mg-m
Zn	0.008–0.05	mg/L
Cr	0.004–0.007	mg/L
Cu	0.001–0.008	mg/L
NO_3–N	0.9–0.11	mg/L
NH_3–N	265–325	mg/L
Total phosphorus	0.348–0.683	mg/L
TSS	3,670–4,280	mg/L
SS	31.7–36.3	mg/L

Scientic Inc., USA). Removals of TOC, color and UV_{254} were calculated using Eq. (2) below:

$$\text{Removal}(\%) = \left(\frac{C_i - C_f}{C_i}\right) \times 100 \tag{2}$$

where C_i and C_f are the initial and final concentrations of the parameters, respectively.

2.2. Experimental design and analytical methodology

MW power setting, PS concentration, and irradiation time were chosen as the critical factors (variables) and designated as X_1, X_2, and X_3, respectively. There were three levels of each factor, and coded as "–" (low level), 0 (center level), and "+" (high level) and these levels were set with appropriate distances apart from the corresponding center levels (Table 2). For example with 70 min as the center point of the irradiation time and the level of irradiation time gap as 60 min, 130 min would be at +1 unit (a 60 min increase from the center point) and 40 min would be at –0.5 unit (a 30 min decrease from the center point). A total of 15 runs were conducted to optimize the level of the chosen factors. The number of experiments (n) required for the development of the BBD was determined below [34]:

$$n = 2k(k-1) + C_0 \tag{3}$$

where k is the number of the factors and C_0 is the number of repetitions of the center point. The details of the experiment design are given in Table 2 and three replicates (no. 9, 11, and 15) were used to evaluate the extent of random experimental errors.

In a BBD optimization process, responses are the running results of experimental combinations relative to the chosen factors. Using the second-order polynomial model to show their relationships, which also includes the linear model, can be expressed as [35]:

$$Y = \beta_0 + \beta_1 X_1 + \beta_2 X_2 + \beta_3 X_3 + \beta_{12} X_1 X_2 + \beta_{13} X_1 X_3 + \beta_{23} X_2 X_3 + \beta_{11} X_1^2 + \beta_{22} X_2^2 + \beta_{33} X_3^2 + \varepsilon \tag{4}$$

where Y is the response; X_1, X_2, and X_3 are the effect of the independent factors; X_{12}, X_{22}, and X_{32} are the square effects; X_1X_2, X_1X_3, and X_2X_3 are the interaction effects; β_1, β_2, and β_3 are the linear coefficients; β_{11}, β_{22}, and β_{33} are the squared coefficients; β_{12}, β_{13}, and β_{23} are the interaction coefficients between the three factors; β_0 is the constant; and ε is the random error, respectively. In order to estimate the β parameters, the experimental matrix notation of the model is shown below [36]:

$$Y = X\alpha + R \tag{5}$$

$$\underbrace{\begin{bmatrix} Y_1 \\ Y_2 \\ \vdots \\ Y_n \end{bmatrix}}_{Y} = \underbrace{\begin{bmatrix} 1 & X_{11} & X_{12} & \cdots & X_{1k} \\ 1 & X_{21} & X_{22} & \cdots & X_{2k} \\ \vdots & \vdots & \vdots & \vdots & \vdots \\ 1 & X_{n1} & X_{n2} & \cdots & X_{nk} \end{bmatrix}}_{X} \underbrace{\begin{bmatrix} \alpha_0 \\ \alpha_1 \\ \vdots \\ \alpha_k \end{bmatrix}}_{\alpha} + \underbrace{\begin{bmatrix} R_1 \\ R_2 \\ \vdots \\ R_n \end{bmatrix}}_{R} \tag{6}$$

where Y is the response vector, X is the design matrix containing the experimental points, α is the vector constituted by the parameters, R is the residual value, n is the number of experiments, and k is the number of factors, respectively. The system of equations was solved using the least-squares method.

A standardized residual plot was used to determine if an observed point was normal or not in statistical analyses. The x-axis of the standardized residual plot corresponded to each point's standardized residual value, while the y-axis corresponded to its normal probability. A normal probability plot of standardized residual was used to recheck the experimental data before statistical analyses. If the standardized residual trend exhibited a normal distribution, all the experimental response points would locate at or cluster around the straight line of 45° from the horizontal line and pass through the origin [24]. If one response point was far away from the standardized line, it meant the statistical trend was not normally distributed. The standardized residual equals to the value of a residual, divided by an estimate of its standard deviation. Standardized residual values were normal in the interval between +2 and -2, which can be helpful in detecting abnormal value. If one response data deviated from all the other observed data, it could be inferred that the absolute value of this response' standardized residual was large (greater than +2 and smaller than -2).

Analysis of variance (ANOVA) is a statistical method commonly used in an RSM data analysis. The main output from an ANOVA study is typically arranged in a table that lists the sources of variation, degrees of freedom, a total sum of squares, and the mean squares. A typical ANOVA table also includes the F and p values with a 95%-confidence level to indicate whether the predictors or factors are significantly related to the response. An adequacy check of the RSM model

Table 2
BBD matrix with three independent factors and the corresponding responses of three parameters

Run no.	Independent factors and coded			Variables and levels			Actual responses (removal, %)			Predicted responses (removal, %)		
	MW power setting; X_1 (W)	PS concentration; X_2 (mM)	Irradiation time; X_3 (min)	X_1 (W)	X_2 (mM)	X_3 (min)	TOC	Color	UV_{254}	TOC	Color	UV_{254}
1	−1	0	+1	325	10	130	74.42	86.78	51.04	71.65	85.29	50.36
2	0	−0.6	−0.5	550	4	40	32.58	09.92	04.80	27.78	13.52	13.57
3	0	+1	−0.5	550	20	40	79.60	89.26	65.98	74.74	83.78	59.17
4	+1	+1	0	775	20	70	75.11	92.29	62.39	78.35	95.26	66.18
5	−1	0	−0.5	325	10	40	32.19	73.00	47.51	41.13	72.84	43.21
6	0	−0.6	+1	550	4	130	42.28	28.37	26.24	48.93	31.93	28.79
7	+1	0	+1	775	10	130	66.64	88.98	53.49	59.76	88.59	56.13
8	0	+1	+1	550	20	130	82.24	96.42	66.10	85.24	94.74	61.59
9	0	0	0	550	10	70	62.75	93.39	52.37	61.39	93.66	52.43
10	+1	−0.6	0	775	4	70	29.94	33.88	40.75	32.87	29.27	31.98
11	0	0	0	550	10	70	62.48	94.21	52.43	61.39	93.66	52.43
12	+1	0	−0.5	775	10	40	55.26	67.77	40.09	55.97	69.81	42.43
13	−1	+1	0	325	20	70	71.21	94.21	66.16	69.82	98.41	73.69
14	−1	−0.6	0	325	4	70	33.27	31.41	27.77	28.49	28.86	25.22
15	0	0	0	550	10	70	58.94	93.39	52.49	61.39	93.66	52.43

is to diagnose the adequacy of the curve that is used to estimate the quadratic regression model [25,35]. The coefficient of determination (R^2) is defined as the percentage of the total variation in the response (Y) that is explained or accounted for by variation in the independent factors. However, when the number of factors increases, the residual decreases and the R^2 value increases [36]. Therefore, one can not depend entirely on the R^2 value to determine the most appropriate regression model. In order to solve this problem, the R^2 value needs to be corrected. After the correction of the R^2 value, any factor is not randomly added into the model to increase the R^2 value. Thus, to obtain a more accurate determination of the regression model, an adjustment on the coefficient of determination (Adj. R^2) is often used to compare the residual per unit degree of freedom [37]. When the factor has a certain degree of contribution to the explanatory ability of the model, the Adj. R^2 value will near the R^2 value. Moreover, Adj. R^2 value should be less than or equal to the corresponding R^2 value. According to the results of Adj. R^2, the applicability of the regression model under different parameters can be compared.

The desirability function was used to simultaneously optimize the responses of all the design factors to translate the functions to a common scale ([0,1]) [25]. The desirability value would be between 0 and 1; and a value closer to 1 indicates a greater chance of achieving the response values. The individual desirability (d) used in the study is [38]:

$$d^{\max} = \begin{cases} 0 & \text{if} \quad Y < \mu \\ \left(\dfrac{Y-\mu}{\mu-\omega}\right)^{S} & \text{if} \quad \mu \le Y \le \omega \\ 1 & \text{if} \quad Y > \omega \end{cases} \tag{7}$$

$$d^{\text{target}} = \begin{cases} \left(\dfrac{Y-\mu}{t-\mu}\right)^{S_1} & \text{if} \quad \mu \le Y \le t \\ \left(\dfrac{Y-\omega}{t-\omega}\right)^{S_2} & \text{if} \quad t \le Y \le \omega \\ 0 & \text{otherwise} \end{cases} \tag{8}$$

where μ, ω and t are the lowest, highest, and target values, respectively. The constants S, S_1, and S_2 have positive values and known as the weights. On the other hand, the composite desirability function (D) was used to simultaneously optimize the responses of all target parameters. The value is also on a ([0,1]) scale as [38]:

$$D = \left(\prod_{n=1}^{k} d_n\right)^{1/k} \tag{9}$$

Once D was defined and the prediction equations for each of the k equations had been computed, it could be used to optimize or rank the predictors.

The experimental design, all the normal distributions of the standardized residuals, the two-dimensional (2D) and response optimization plots (including the desirability function) of the BBD quadratic model and the ANOVA analysis were done by using the Minitab 17.0 software. In this study, the three-dimensional (3D) response surface plots were done by using the SigmaPlot 12.0 software. Fig. 1 illustrates the schematic diagram of this study.

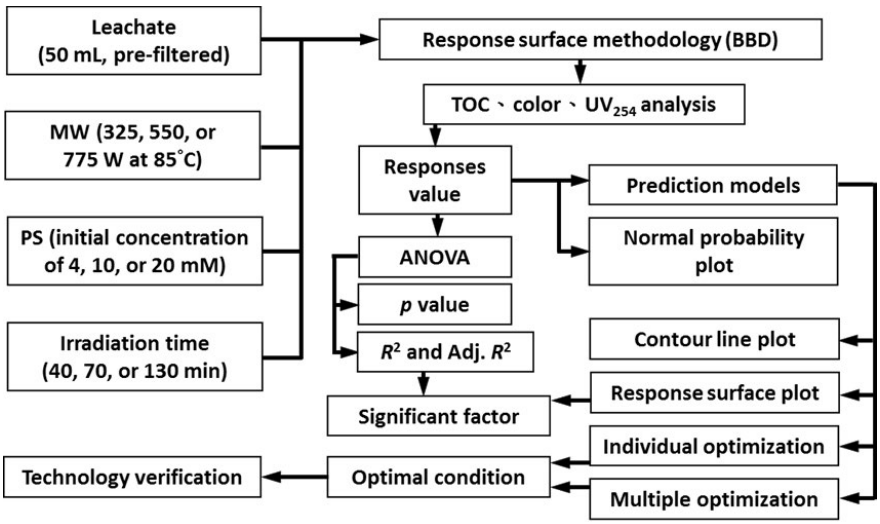

Fig. 1. Schematic diagram of the MW-enhanced oxidation process and optimization by response surface methodology (BBD).

3. Results and discussion

3.1. Optimization by using the BBD

MW power setting, initial PS concentration, and irritation time are the most important factors of MW-assisted oxidation. BBD analysis was applied in the experimental design of this study while the Minitab software was applied in the statistical analyses of factors' interaction. Removals of TOC, color, and UV_{254} were chosen to be the responses, and the experimental results are tabulated in Table 2. Using the data shown in Table 2 and the second-order polynomial model of Eq. (4), the results of the regression analysis are shown below:

$$Y_{TOC} = -73.7 + 0.1762X_1 + 6.43X_2 + 0.768X_3 + 0.00058X_1X_2 - 0.00066X_1X_3 - 0.0074X_2X_3 - 0.000111X_1^2 - 0.1466X_2^2 - 0.00082X_3^2 \quad (10)$$

$$Y_{color} = -117.1 + 0.0759X_1 + 19.0X_2 + 1.392X_3 - 0.0005X_1X_2 + 0.000156X_1X_3 - 0.00518X_2X_3 - 0.000076X_1^2 - 0.5887X_2^2 - 0.00737X_3^2 \quad (11)$$

$$Y_{UV_{254}} = -37.9 - 0.03X_1 + 8.39X_2 + 0.876X_3 - 0.00198X_1X_2 + 0.000162X_1X_3 - 0.0089X_2X_3 + 0.000038X_1^2 - 0.1707X_2^2 - 0.00447X_3^2 \quad (12)$$

where Y_{TOC}, Y_{color}, and $Y_{UV_{254}}$ are the values of the above functions (10) to (12), respectively; while each function is composed of the three factors: MW power setting (X_1), initial PS concentration (X_2), and irritation time (X_3).

Fig. 2 illustrates the normal probability plots of standardized residuals in the MW-assisted oxidation process. All the three parameters' responses (TOC, color, and UV_{254} removals) were close to their corresponding straight lines, which implies that most responses are normally distributed and their standardized residuals values on X-axis are in the interval between +2 and –2. Besides, the rationality of all the experimental results could be assessed in advance by these analyses of normal probability plots of standardized residuals. As shown in Table 2, there are a total of 15 sets of responses in the BBD matrix, which includes three independent factors (MW power setting (X_1), initial PS concentration (X_2), and irritation time (X_3)) and their corresponding responses. The center of the BBD matrix was at the point (550 W, 10 mM, and 70 min), and all the predicted analyses of Table 2 were conducted and calculated by using Eqs. (9) to (11). In statistical analysis, if the Pearson correlation coefficient (r) is larger than 0.95, it implies a highly positive correlation among the observed data. By looking at the column of actual response and that of predicted response, the Pearson correlation coefficients of TOC, color, and UV_{254} were 0.97, 0.995, and 0.959, respectively. They imply that good relationship between the actual and the predicted values.

3.2. ANOVA statistical analysis

In an ANOVA statistical analysis, if the probability p-value is less than 0.05 (~0.0001), it means that if is significant at a >95% probability level. Table 3 tabulates the ANOVA test results using the RSM with the model term, linear terms (X_1, X_2, X_3), squared terms (X_1^2, X_2^2, X_3^2), and interaction terms (X_1X_2, X_1X_3, X_2X_3) vs. three parameters (TOC, color, and UV_{254}). Since all the p-values are less than 0.05 in the model term, the results indicate that the removals of three parameters are all significant and effective, independent of the models being linear terms, squared terms, or interaction terms [39].

The linear terms demonstrate the effect of a single factor on each parameter. The smaller the p-value is; the more influence it has on the removal of the parameter. For the case of the X_2 model, the p -values of TOC, color, and UV_{254} parameters were less than 0.05, which implies that X_2 has the most significant effect on pollutant removals. For the case of X_1 model, the results show that the p-values of TOC and color parameters were larger than 0.05, which implies that the

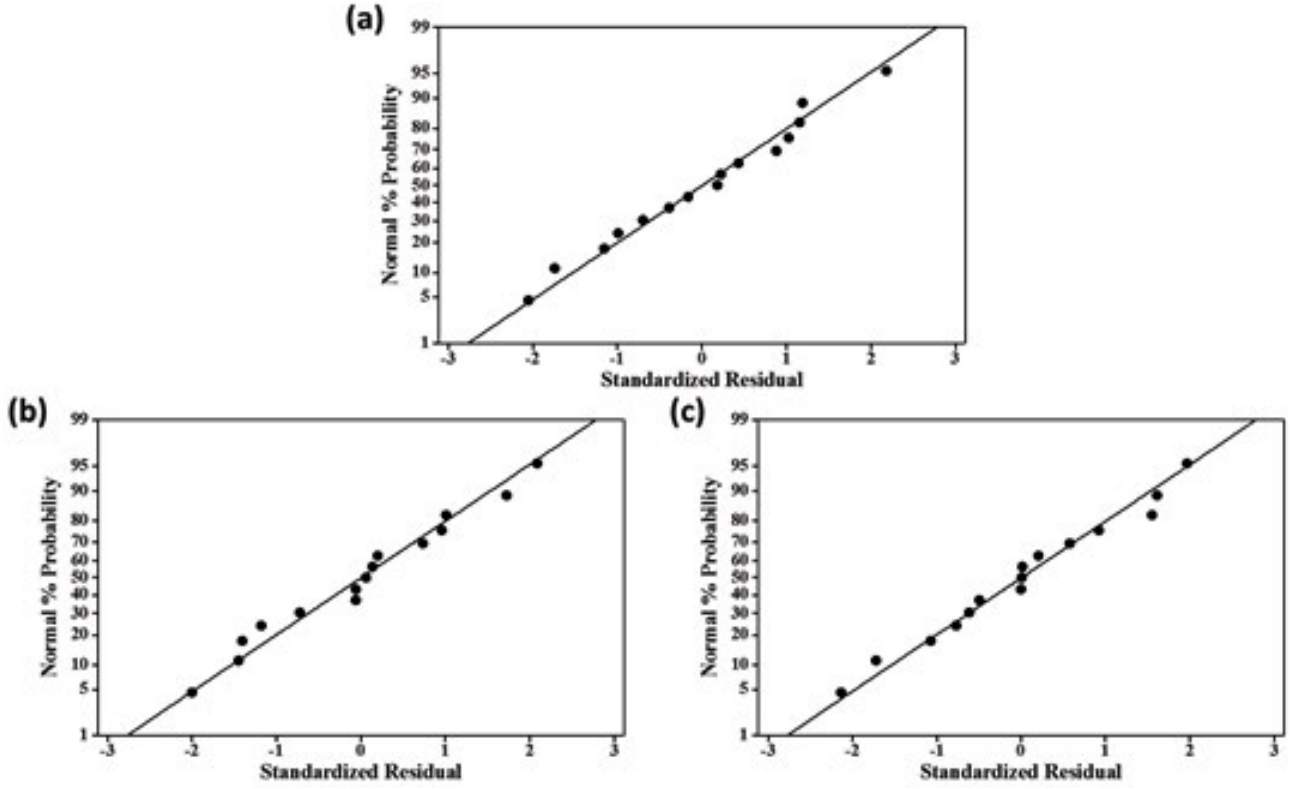

Fig. 2. Normal probability plots of the standardized residuals for removals of (a) TOC, (b) color, and (c) UV_{254}.

Table 3
Analysis of variance (ANOVA) test for response surface quadratic model for three parameters removals of leachate

		TOC				Color				UV_{254}			
Source	[a]DF	[b]Adj. SS	[c]Adj. MS	*F*	*p*	Adj. SS	Adj. MS	*F*	*p*	Adj. SS	Adj. MS	*F*	*p*
Model	9	4,578.73	508.75	8.83	0.014	12,468.6	1,385.4	57.83	<0.0001	3,807.16	423.02	6.29	0.028
X_1–MW power setting (W)	1	1.88	1.884	0.03	0.864	1.1	1.08	0.05	0.840	47.89	47.887	0.71	0.437
X_2–PS concentration (mM)	1	801.89	801.885	13.91	0.014	6,882.7	6,882.73	287.3	<0.0001	915.47	915.469	13.62	0.014
X_3–Irradiation time (min)	1	247.22	247.221	4.29	0.093	441.4	441.41	18.43	0.008	269.42	269.415	4.01	0.102
X_1^2	1	117.21	117.213	2.03	0.213	55.1	55.09	2.3	0.19	13.47	13.474	0.2	0.673
X_2^2	1	277.62	277.62	4.82	0.08	4,477.4	4,477.44	186.9	<0.0001	376.38	376.38	5.6	0.064
X_3^2	1	7.72	7.723	0.13	0.729	618.3	618.28	25.81	0.004	227.39	227.387	3.38	0.125
X_1X_2	1	4.43	4.425	0.08	0.793	3.3	3.28	0.14	0.727	52.33	52.335	0.78	0.418
X_1X_3	1	188.36	188.365	3.27	0.13	10.6	10.57	0.44	0.536	11.3	11.299	0.17	0.699
X_2X_3	1	30.81	30.813	0.53	0.497	15.1	15.09	0.63	0.463	44.48	44.484	0.66	0.453
R^2		0.94				0.99				0.92			
Adj. R^2		0.83				0.97				0.77			

[a]DF: degree of freedom; [b]Adj. SS: an adjusted sum of squares; [c]Adj. MS: adjusted mean of squares.

effects of X_1 were insignificant on TOC and color removals. For the case of the X_3 model, the effects of X_3 were insignificant on TOC and UV_{254} removals, but significant on color removal. The order of significance is as follows: $X_2 > X_3 > X_1$.

The squared terms demonstrate the additional effects of each factor. These additional effects could be observed from the bend phenomena on the plane response curves of the second-order polynomial model. One of the advantages

of the RSM model is that it is more convenient to observe the relationship between factors and parameters. A smaller *p*-value has a larger curvature on the plane response curve by means of a significant bend phenomenon. For example, in the case of the X_2^2 model shown in Table 3, the *p*-values are smaller among these three parameters; in other words, X_2 has a more significant curvature on the plane response curve when compared to the other two factors.

The interaction terms are usually used to evaluate if there is an interaction between two factors. As shown in Table 3, most interaction terms (X_1X_2, X_1X_3, X_2X_3) have larger *p*-values, and the results imply that interaction effects are less significant in the MW oxidation process. Similar to the cases of the squared terms, a smaller *p*-value has a larger curvature on the plane response curve. For the case of the X_1X_3 model, the *p*-value is 0.13, and the curvature of TOC response is the largest among the three parameters. Comparatively, the curvature of TOC response has the smallest *p*-value of 0.793 in the case of the X_1X_2 model. In summary, the results shown in Table 3 indicate that the key effects on TOC, color, and UV_{254} removals are due to each factor by itself, not the interactions among them.

Table 3 also shows the Adj. R^2 values of TOC, color, UV_{254} parameters are 0.83, 0.97, and 0.77, respectively. The Adj. R^2 values are smaller than their corresponding R^2 values. From a statistic point of view, its performance on the color removal (Adj. $R^2 = 0.97$) is better than those of TOC (Adj. $R^2 = 0.83$) and UV_{254} (Adj. $R^2 = 0.77$), which also implies that the RSM model is more suitable in predicting the color removals.

3.3. Analysis of contour-line

The Minitab software was used to plot the 2D contour-line to model the relationship between the three factors and the three parameters. The parameters' removals could be calculated by the density of both contours in Fig. 3 to observe their spatial gradient changes. As shown in Table 3, the ANOVA test indicates that X_2 in the linear terms has the largest significance with $p < 0.05$, X_1 vs. X_3 was chosen to plot the 2D contour-line under three different X_2 of 4, 10, and 20 mM. It should be noted that the right-hand side of the dotted line in Fig. 3 indicates the modeling errors, and these errors would never happen in real situations. In other words, removal rates would never decrease with increases of X_2.

Fig. 3a illustrates the cases of TOC removal rates under various X_1 and X_3. The TOC removal efficiencies of three X_2 were weak at lower MW power and shorter illumination time settings. Only when both MW power and irradiation time increased, the TOC removals rose. Under the same condition, the average TOC removal rates in 20 mM (65%–85%) were greater (e.g., twice or so) than those in 4 mM (20%–50%). Chou et al. [30] mentioned that more intensive MW energy input would cause more PS ions being heat-catalyzed to initiate sulfate-free radical chain reactions to cause the decay of PS ions sooner. This could explain why TOC removal rates only slightly increased with increasing MW powers as shown in Fig. 3a.

Fig. 3b illustrates the color removal rates under various X_1 and X_3. Gaps in removal rates show obvious dense/sparse changes and isopleth contour-lines have a nearly-vertical arrangement. It indicates that color removal rates varied significantly with irradiation times. In addition, in the cases of higher and lower MW power settings with the same irradiation time, color removal was 75% at PS concentration of 10 mM and near 100% at 20 mM, respectively. It has been reported in the literature that the long-chain structures and unsaturated groups of colors could be decomposed under higher PS concentrations [40]. When the X_2 was less than 4 mM, color removals were insignificant.

Fig. 3c illustrates UV_{254} removal rates under various X_1 and X_3. The removals of organic compounds with double bonds in the leachate were less apparently affected by X_2. Removals of some UV_{254} require a longer irradiation time and higher PS concentrations. As shown in Fig. 3c, UV_{254} removals increased slightly with increasing PS concentrations. In the case of 20 mM X_2, the UV_{254} removal rates were in the range of 60%–72%, which were almost twice those of 4 mM X_2, only 20%–35%.

3.4. Analysis of response surface

Eqs. (9) and (10) were used to plot three 3D response surfaces of X_1, X_2, and X_3, with the center of the BBD, set at 550 W, 10 mM, and 70 min, respectively. As shown in Figs. 4a–c, the 3D response surfaces are useful to provide important information about the optimal settings for removals.

In the case of X_1 at 550 W (Fig. 4a), the results show that the TOC, color, and UV_{254} removals were 86% (20 mM, 130 min), 100% (lots of points), and 70% (19 mM, 130 min), respectively. In addition, color removals were nearly complete decomposition and stable at high PS concentrations. It should be noted that lots of points in the 3D response surfaces show that the color removals were greater than 100%, which are impossible [40]. They actually should be viewed as complete decomposition. It was also found that TOC and UV_{254} removals increased with the PS concentration and irradiation time. Fig. 4a illustrates that X_2, exerted a more significant effect on removals than X_3, as indicated by the 3D response surfaces' curvatures.

For X_2 of 10 mM (Fig. 4b), the average color removal was greater than 70%; it implies that most long-chain structures and unsaturated groups of color compounds could be decomposed with a PS concentration of 10 mM. The results show that the maximum TOC, color, and UV_{254} removals were 73% (433 W, 130 min), 99% (566 W, 97 min), and 60% (775 W, 102 min), respectively. Fig. 4b also shows that TOC, color, and UV_{254} removals increased slightly with X_1 and X_3, due to self-scavenging of free radicals under longer irradiation times and higher MW powers [29]. It is plausible that X_2 is a more significant factor than X_1 and X_3. From the increasing trend of 3D response surfaces' curvatures, it indicates that the effect of X_3 on removal was only slightly greater than that of X_1.

For X_3 of 70 min (Fig. 4c), the results show that the maximum TOC, color, and UV_{254} removals were 81% (638 W, 20 mM), 100% (lots of points), and 74% (325 W, 20 mM), respectively. It should be noted that the color removals had a well and stable performance at this irradiation time coupled with higher PS concentrations. Under lower PS

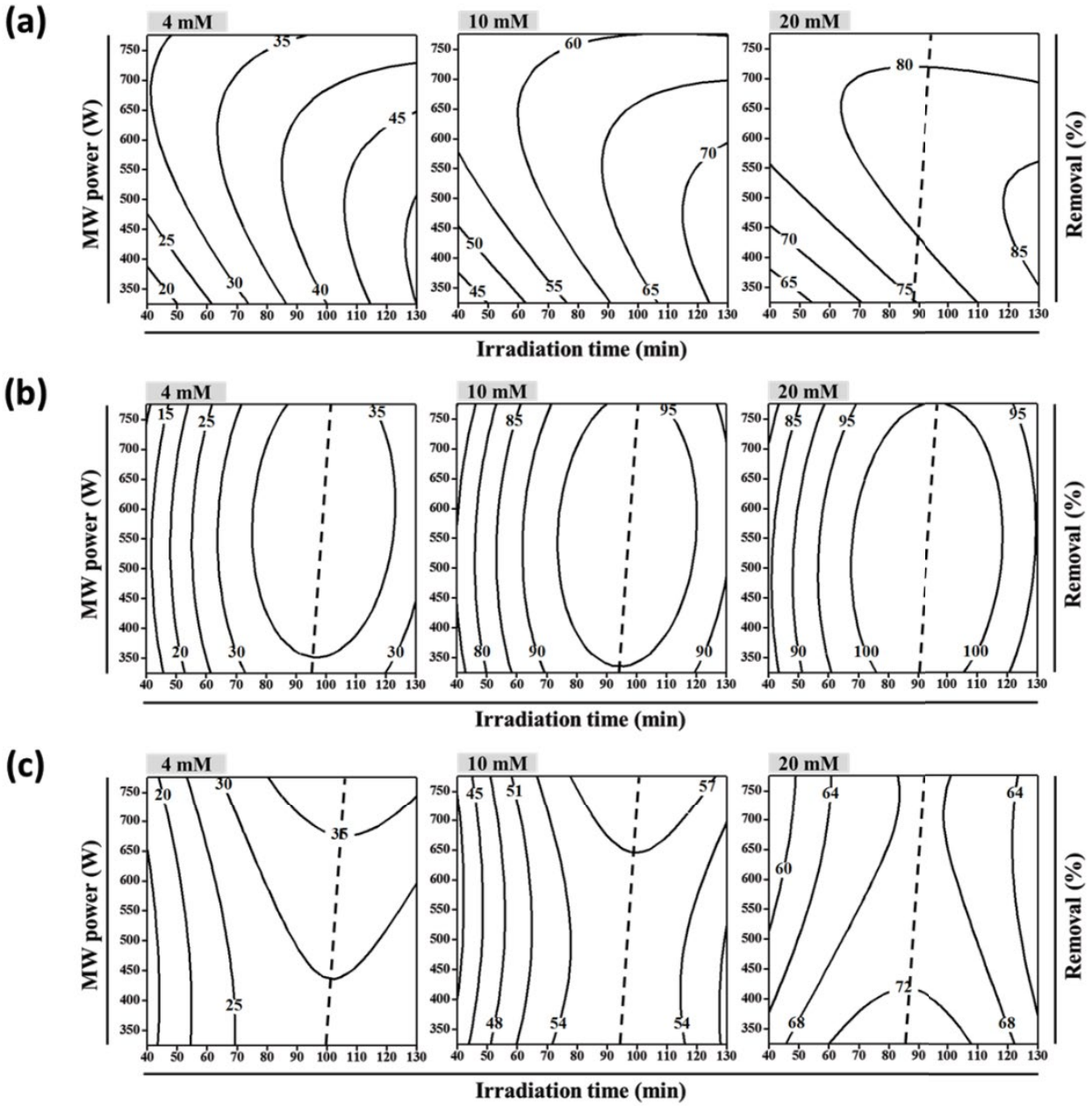

Fig. 3. 2D contour-line plots of the quadratic model for removals of (a) TOC, (b) color, and (c) UV_{254} in different initial PS concentrations (4, 10, 20 mM) at 85°C.

concentrations, TOC, color, and UV_{254}, the removals were the worst. From the increasing trend of 3D response surfaces' curvatures, it indicates that the effect of X_2 (fast increasing) on removal was greater than that of X_1, especially in color removal.

All the results have been discussed by using the fixed center factor method. If three factors were discussed by the individual parameters' point of view, the analysis results were as follows. For the case of TOC removal in Figs. 4a–c as an example, the maximum value in each figure minus the corresponding minimum value is defined as difference value. The difference values of Figs. 4a–c were 58% (i.e., 86%–28%), 32% (i.e., 73%–41%), and 52% (i.e., 81%–29%), respectively. Fig. 4b has the smallest difference of 32%, which means that the *x*-axis (X_3) and *y*-axis (X_1) had an insignificant effect on the TOC parameter. The variation of TOC removals was the smallest at a fixed X_2. In other words, X_2 was a more significant factor in the TOC removal than X_1 and X_3. Similarly, for the cases of color removal in Figs. 4a–c, the differences were 86% (i.e., 100%–14%), 29% (i.e., 99%–70%), and 71% (i.e., 100%–29%), respectively. Similarly, X_2 was a more significant factor on color removal than the other two. For the case of UV_{254} removal in Figs. 4a–c, the differences between Figs. 4a–c were 56% (i.e., 70%–14%), 19% (i.e., 60%–41%),

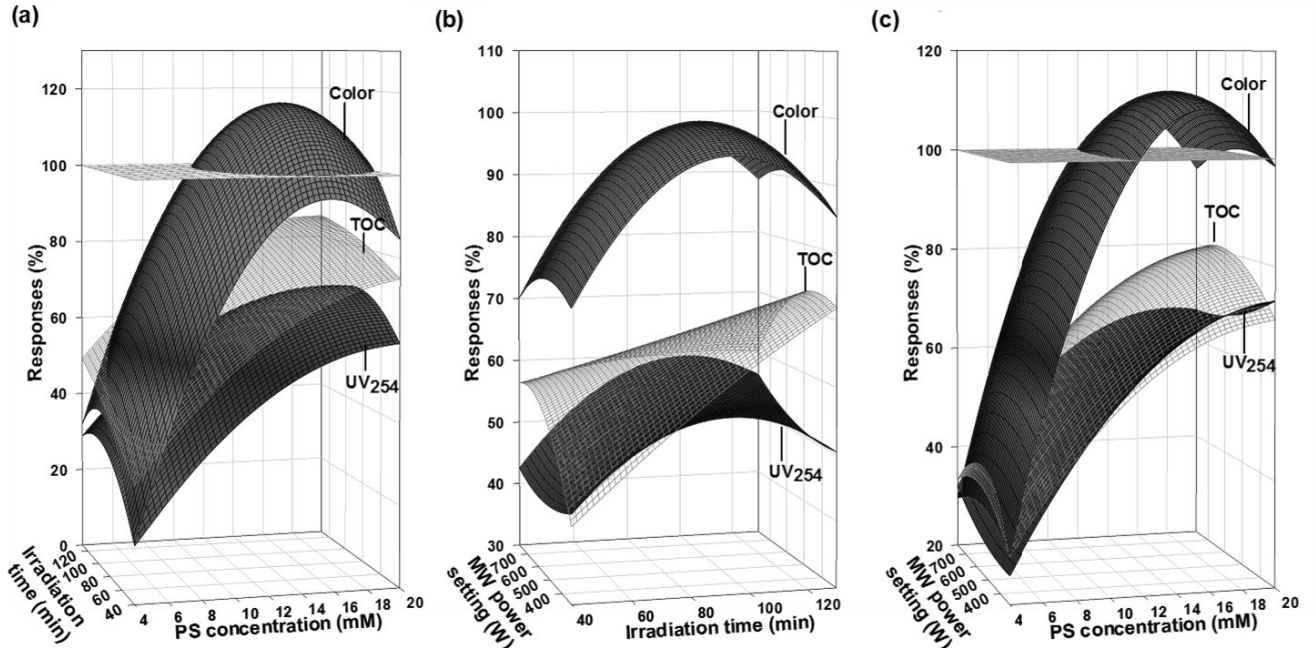

Fig. 4. 3D response surface plots of a quadratic model at 85°C for removals at (a) MW power setting = 550 W, (b) PS concentration = 10 mM, and (c) irradiation time = 70 min.

and 49% (i.e., 74%–25%), respectively. Similarly, X_2 was a more significant factor in the UV_{254} removal.

As shown in Table 3, the more significant factor could be derived from the *p*-value (PS factor, X_2) of the ANOVA linear terms. Otherwise, 3D response surfaces' curvatures could be obtained by the ANOVA interaction terms. Compared a comparison with Table 3 and Fig. 4, TOC had the greatest curvature change in X_1X_3 with $p = 0.13$, which implies that the TOC response surfaces in Fig. 4b had a maximum curvature phenomenon and a minimum *p*-value. Most RSM literature offered a few discussions on the relationships between 3D response surfaces' curvature and ANOVA [24–28].

3.5. Response optimization

Fig. 5 illustrates the response optimizations of TOC, color, and UV_{254} removals from the single– and multiple–parameters analysis by using the Minitab software. In Fig. 5, the rows indicate whether TOC, color, or UV_{254} removals are the maximum or the target values; while the columns are the response optimizations of X_1, X_2, and X_3, respectively. Besides, the gray vertical lines are the optimal operational lines; the gray number values with square brackets are optimal operational values. The gray horizontal dotted lines and *Y*-values in Fig. 5 are optimal response values. The letters *d* and *D* are for the desirability and composite desirability values, respectively. The results of Nayak and Pal [25] indicated that a higher"*d*" value could be employed effectively for the estimation of optimal influences of the independent treating parameters. There are three response values (TOC, color, and UV_{254}) and their corresponding desirability function values *D* [Eqs. (6) and (7)]. It has been reported that the bending level of curves depending on the *p*-values in Table 3, where a larger curvature corresponds to a smaller *p*-value. In other words, the optimal response reflects an increased curvature of the response surface, and this finding was not shown in our previous studies [29–31].

Fig. 5a shows the response optimizations of X_1, X_2, and X_3; they were 456.8 W, 19.5 mM, and 130 min, respectively, for the highest TOC removal rate of $Y = 86.22\%$ with $d = 0.937$. Higher TOC removals relied on increasing free radicals concentrations with higher PS concentrations, longer oxidation times, and longer MW irradiation times. These findings correspond well to those reported by Chou et al. [29]. Observed TOC response curve, the setting values on both sides of the inflection point were smaller than 86.22%, and it had a linear proportion between TOC removals and irritation time ($X_3 < 130$ min). For the case of color removals, the response optimizations of three factors were 752.3 W, 15.2 mM, and 54.5 min, with the highest color removal rate of $Y = 99.99\%$ with $d = 0.999$. It should be noted that the points above the dotted line indicating a complete color removal. For the color response curves, the setting values on both sides of the inflection point were smaller than 100%, indicating that X_1 had weak influences on color removals. For the case of UV_{254} removals, the response optimizations of three factors were 325 W, 20 mM, and 83.6 min, with the highest UV_{254} removal rate of $Y = 74.55\%$ with $d = 1.0$. Under the operational setting of $X_2 = 20$ mM and $X_3 = 83.6$ min, the response curve of X_1 had a minimum difference value in remove rate (6.49%), that is 74.55% at 325 W minus 68.06% at 740 W. In other words, X_1 had weak influences on UV_{254} removals, whereas X_2 was more important on UV_{254} removals. The response curve of X_2 had the largest difference value of removal, and this curve rose with increasing PS concentrations.

The ultimate goal of the RSM was to provide the optimization for single– or multiple–parameters. As shown in Fig. 5b, the common optimizations of three factors were

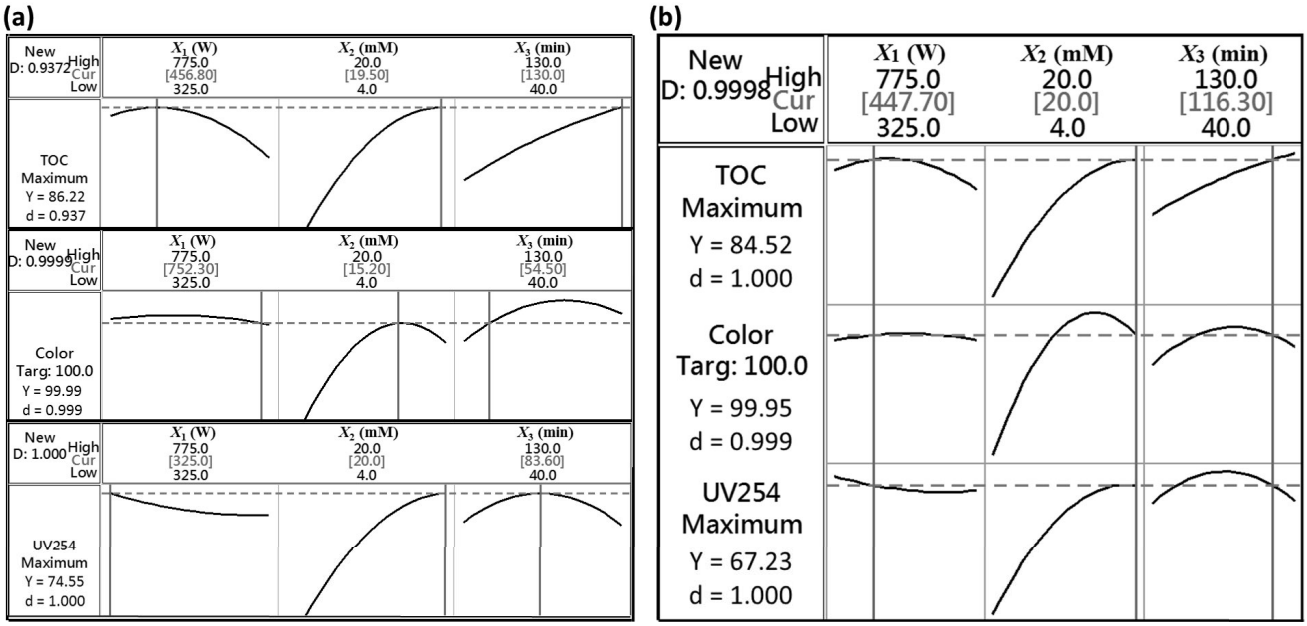

Fig. 5. (a) Individual and (b) multiple optimal conditions in the response curves for removals at 85°C with the Box–Behnken design (High: highest value; Cur: current value (optimal value); Low: lowest value; *d*: desirability value; *D*: composite desirability value).

448 W, 20 mM, and 116.3 min. The results corresponded to removals of 84.52, 100, and 67.23% of TOC, color, and UV_{254}, respectively. Based on Eq. (8), the optimal results occurred when the single desirability function value (*d*) and common desirability function values (*D*) were both close to 1.0. If the results of multiple optimizations compared with the results of single optimization, TOC and UV_{254} removals decreased 1.7% (i.e., 86.22%–84.52%) and 7.32% (i.e., 74.55%–67.23%), respectively, while color removals showed little variations.

3.6. An offer of the technology verification in optimal conditions

According to Kirmizakis et al. [39], their study provided the optimal treatment conditions for removals of COD in the landfill leachate with the assisted design tool of RSM successfully and proved that the RSM theory was applicable for wastewater treatment. Compared to our research group's previous microwave studies [29–31], the highlight of this study is to use statistical verification to explore the feasibility of previous experimental results. The main treatment technology is the MW-enhanced oxidation process, with simultaneous use of the RSM to infer the optimal MW power settings. Under the optimal operation settings, PS could release more sulfate radicals and provide sufficient oxidizing capability to remove the target compounds effectively in the MW-enhanced oxidation process. Unnecessary oxidant overdose was avoided and better pollutant removals (color, long-chain and unsaturated organic compounds) were achieved in the RSM-forecasted condition. Due to the limitations of the instrument settings, the MW power setting is adjusted to an integer value for experimentation in Table 4. In the case of single parameter optimization, 79.48% of TOC removal was achieved under the settings of 457W, 19.5 mM, and 130 min; near 100% of color removal was achieved under the settings of 752 W, 15.2 mM, and 54.5 min; and 68.39% of UV_{254} removal was achieved under the settings of 325 W, 20 mM, and 83.6 min. From the results of the RSM modeling, color removals showed less differences when compared to the actual experimental results. It implied that color most compounds included long-chain structures and unsaturated groups could be decomposed completely in the optimal operating conditions. Although larger relative differences were found in TOC and UV_{254} predictions, they were less than 10% and it also means this treatment technology is valuable. MW oxidation treatment could mineralize most TOCs in the leachate; nevertheless, it is still difficult to destroy all the organic compounds completely; even if the operational settings were optimal. However, organic compounds with double bonds could be readily degraded by sulfate radicals and persulfate oxidation. The results are comparable to those of Chou et al. [31] and Ishak et al. [5], while the TOC and color removals of this study are better than those of Saleem et al. [6] and Yusoff et al. [4], respectively. In the case of multiple–parameter optimizations, 78.81% of TOC removal, near 100% of color removal, and 66.44% of UV_{254} removal were found under the settings of 448W, 20 mM, and 116.3 min. These results show very small differences from the color and UV_{254} predictions, whereas a larger difference in TOC prediction. In addition, the color removals were higher in the quadratic regression analysis of the RSM for both single– or multiple–parameters optimization. The high MW power settings and excessive additions of PS oxidants reduced the target compound removals. Compared to those in our previous studies [29,31], MW power settings were lower with lower oxidant concentrations, but with a longer irradiation time; and these operating conditions led to better removal efficiencies in this study.

Under this treatment technology, most experimental trends showed that the predicted results were close to the corresponding actual results. The results show that if a

Table 4
Removals under optimal conditions from the model prediction and the technology verification experiment

	MW power setting (W)	PS concentration (mM)	Irradiation time (min)	Predicted values (%)	Experimental values (%)	Relative error (%)
Individual optimal operating conditions						
TOC	457*	19.5	130	86.22	79.48	8.48
Color	752*	15.2	54.5	99.99	100	–0.01
UV_{254}	325	20	83.6	74.55	68.39	9.01
Multiple optimal operating condition						
TOC				84.52	78.81	7.25
Color	448*	20	116.3	99.95	100	–0.05
UV_{254}				67.23	66.44	1.19

*The MW power settings have fear rounded to 457, 752, and 448 W, respectively.

multi–parameter was considered as the optimal removal condition, the removals in both predicted and actual values of TOC and UV_{254} would be decreased than those of single–parameter' optimization. If the optimal removal condition efficiency of a single–parameter was considered, the results of this study suggest that a single optimized treating condition in the Minitab software should be chosen.

3.7. Analysis of treatment technology cost

The treatment cost is a major issue for MW-enhanced oxidation processes. In addition to capital costs, the operational costs of electricity and chemicals should be considered. In each experiment, eight 50 mL bottles were used to treat 400 mL of the leachate at a time. Taking the multi-parameter results as an example, 20 mM of PS was used, that is 0.243 g of PS in a 50 mL sample or 4.8571 kg of PS per m^3 of leachate. With a cost of USD $1.33 per kg of PS, the chemical cost would be USD $6.48/$m^3$ of leachate. With regards to electricity, in the case of MW 448 W power setting with an irradiation time of 116.3 min, the power consumption would be 0.8684 kWh for 400 mL; that is 2,170.9 kWh for 1 m^3 of leachate. With an electricity cost of USD $0.082/kWh, the cost of electricity would be USD $177.2/$m^3$ of leachate. Consequently, the combined chemical and electricity cost was roughly USD $183.6/$m^3$ of leachate on the laboratory scale. There is a biogas power generation system in Sanjuku Landfill, which could provide electricity to the treatment system, so the cost could be cheaper.

4. Conclusion

This study successfully used MW-assisted PS oxidation to treat landfill leachate and amalgamated with the RSM and the ANOVA statistical analysis to find the optimal operational settings. With an offer of the technology, the optimum removals of TOC, color, and UV_{254} were 79.48%, near 100%, and 68.39%, respectively. Initial PS concentrations had significant influences on TOC, color, and UV_{254} removals. RSM helps this treatment technology to find the best removal efficiency and analyze the information about the treatment technology. Higher R^2 and Adj. R^2 values were observed in the quadratic regression analysis and the ANOVA analysis. ANOVA table and 3D response surfaces are useful to derive useful information on optimal settings for removals. Each parameter' removals and its relationship among experimental factors could be clearly observed in the 3D response surfaces of the RSM inference. For all MW oxidation experimental runs, color removals were higher than those of TOC and UV_{254}. This study offer efficiency the technology in treating landfill leachate and not only indicates the optimal conditions through the BBD design and the ANOVA test, but also provides an important consideration for selecting single– or multi–parameter removal efficiency, operating conditions, and the cost assessment.

Acknowledgment

The TOC analyzer and the UV-Vis spectrophotometer were provided by the Department of Water Resources and Environmental Engineering, Tamkang University. We would like to thank Professors Tau Being Hsu and Chi-Wang Li for their valuable comments and assistance.

References

[1] J. Zhao, X.Q. Lu, J.H. Luo, J.Y. Liu, Y.F. Xu, A.H. Zhao, F. Liu, J. Tai, G.R. Qian, B. Peng, Characterization of fresh leachate from a refuse transfer station under different seasons, Int. Biodeterior. Biodegrad., 85 (2013) 631–637.
[2] L. Miao, G. Yang, T. Tao, Y. Peng, Recent advances in nitrogen removal from landfill leachate using biological treatments–a review, J. Environ. Manage., 235 (2019) 178–185.
[3] C. Yuan, C. Lu, Y. Ma, Y. Wang, Y. Xie, K. Zhang, Y. Wang, L. Lv, X. Feng, T. Zhu, A novel method to treat old landfill leachate combining multi-stage biological contact oxidation (MBCO) and single-stage autotrophic nitrogen removal using anammox and partial nitrification (SNAP), Chem. Eng. J., 359 (2019) 1635–1643.
[4] M.S. Yusoff, H.A. Aziz, M.F.M.A. Zamri, A.Z. Abdullah, N.E.A. Basri, Floc behavior and removal mechanisms of cross-linked *Durio zibethinus* seed starch as a natural flocculant for landfill leachate coagulation-flocculation treatment, Waste Manage., 74 (2018) 362–372.
[5] A.R. Ishak, F.S. Hamid, S. Mohamad, K.S. Tay, Stabilized landfill leachate treatment by coagulation-flocculation coupled with UV-based sulfate radical oxidation process, Waste Manage., 76 (2018) 575–581.
[6] M. Saleem, A. Spagni, L. Alibardi, A. Bertucco, M.C. Lavagnolo, Assessment of dynamic membrane filtration for biological

treatment of old landfill leachate, J. Environ. Manage., 213 (2018) 27–35.
[7] L. Azzouz, N. Boudjema, F. Aouichat, M. Kherat, N. Mameri, Membrane bioreactor performance in treating Algiers' landfill leachate from using indigenous bacteria and inoculating with activated sludge, Waste Manage., 75 (2018) 384–390.
[8] Q. Xu, G. Siracusa, S. Di Gregorio, Q. Yuan, COD removal from biologically stabilized landfill leachate using advanced oxidation processes (AOPs), Process Saf. Environ. Prot., 120 (2018) 278–285.
[9] N. Savchuk, P. Krizova, Membrane, AOPs processes—their application and comparison in treatment of wastewater with high organics content, Desal. Water Treat., 56 (2015) 3247–3251.
[10] E.M. Kiley, V.V. Yakovlev, K. Ishizaki, S. Vaucher, Applicability study of classical and contemporary models for effective complex permittivity of metal powders, J. Microwave Power Electromagn. Energy, 46 (2012) 26–38.
[11] T. Yousefi, S.A. Mousavi, M.Z. Saghir, B. Farahbakhsh, An investigation on the microwave heating of flowing water: a numerical study, Int. J. Therm. Sci., 71 (2013) 118–127.
[12] V. Abdelsayed, D. Shekhawat, M.W. Smith, D. Link, A.E. Stiegman, Microwave-assisted pyrolysis of Mississippi coal: a comparative study with conventional pyrolysis, Fuel, 217 (2018) 656–667.
[13] Y.F. Huang, P.T. Chiueh, W.H. Kuan, S.L. Lo, Microwave pyrolysis of lignocellulosic biomass: heating performance and reaction kinetics, Energy, 100 (2016) 137–144.
[14] N. Van Suc, Removal of direct dyes from aqueous solution by adsorption onto the mangrove charcoal activated by microwave-induced phosphoric acid, Desal. Water Treat., 118 (2018) 304–313.
[15] C. Yin, J. Cai, L. Gao, J. Yin, J. Zhou, Highly efficient degradation of 4-nitrophenol over the catalyst of Mn_2O_3/AC by microwave catalytic oxidation degradation method, J. Hazard. Mater., 305 (2016) 15–20.
[16] C.M. Park, J. Heo, D. Wang, C. Su, Y. Yoon, Heterogeneous activation of persulfate by reduced graphene oxide–elemental silver/magnetite nanohybrids for the oxidative degradation of pharmaceuticals and endocrine-disrupting compounds in water, Appl. Catal., B, 225 (2018) 91–99.
[17] D. Wu, X. Li, J. Zhang, W. Chen, P. Lu, Y. Tang, L. Li, Efficient PFOA degradation by persulfate-assisted photocatalytic ozonation, Sep. Purif. Technol., 207 (2018) 255–261.
[18] M. Arbabi, M. Sadeghi, A. Fadaei, S. Hemati, S. Shahsavan, Evaluation of sulfadiazine (SDZ) removal from wastewater by persulfate activated with iron sulfate, Desal. Water Treat., 113 (2018) 160–164.
[19] G. Fan, L. Cang, H.I. Gomes, D. Zhou, Electrokinetic delivery of persulfate to remediate PCBs polluted soils: effect of different activation methods, Chemosphere, 144 (2016) 138–147.
[20] G. Fang, W. Wu, C. Liu, D.D. Dionysiou, Y. Deng, D. Zhou, Activation of persulfate with vanadium species for PCBs degradation: a mechanistic study, Appl. Catal., B, 202 (2017) 1–11.
[21] D.M. Stanbury, Reduction potentials involving inorganic free radicals in aqueous solution, Adv. Inorg. Chem., 33 (1989) 69–138.
[22] R. Xie, J. Ji, K. Guo, D. Lei, Q. Fan, D. Y. Leung, H. Huang, Wet scrubber coupled with UV/PMS process for efficient removal of gaseous VOCs: roles of sulfate and hydroxyl radicals, Chem. Eng. J., 356 (2019) 632–640.
[23] A. Fernandes, P. Makoś, G. Boczkaj, Treatment of bitumen post oxidative effluents by sulfate radicals based advanced oxidation processes (S-AOPs) under alkaline pH conditions, J. Cleaner Prod., 195 (2018) 374–384.
[24] J.E. Silveira, J.A. Zazo, G. Pliego, E.D. Bidóia, P.B. Moraes, Electrochemical oxidation of landfill leachate in a flow reactor: optimization using response surface methodology, Environ. Sci. Pollut. Res., 22 (2015) 5831–5841.
[25] A.K. Nayak, A. Pal, Rapid and high-performance adsorptive removal of hazardous acridine orange from aqueous environment using *Abelmoschus esculentus* seed powder: single- and multi–parameter optimization studies, J. Environ. Manage., 217 (2018) 573–591.
[26] R. Shokoohi, M.T. Samadi, M. Amani, Y. Poureshgh, Optimizing laccase-mediated amoxicillin removal by the use of Box–Behnken design in an aqueous solution, Desal. Water Treat., 119 (2018) 53–63.
[27] S.L. Wong, N. Ngadi, N.A.S. Amin, T.A.T. Abdullah, I.M. Inuwa, Pyrolysis of low-density polyethylene waste in subcritical water optimized by response surface methodology, Environ. Technol., 37 (2016) 245–254.
[28] C.Y. Wu, W.B. Lui, J. Peng, Optimization of extrusion variables and maleic anhydride content on biopolymer blends based on poly (hydroxybutyrate-co-hydroxyvalerate)/poly (vinyl acetate) with tapioca starch, Polymers, 10 (2018) 827.
[29] Y.C. Chou, S.L. Lo, J. Kuo, C.J. Yeh, A study on microwave oxidation of landfill leachate—contributions of microwave-specific effects, J. Hazard. Mater., 246 (2013) 79–86.
[30] Y.C. Chou, S.L. Lo, J. Kuo, C.J. Yeh, Derivative mechanisms of organic acids in microwave oxidation of landfill leachate, J. Hazard. Mater., 254 (2013) 293–300.
[31] Y.C. Chou, S.L. Lo, J. Kuo, C.J. Yeh, Microwave-enhanced persulfate oxidation to treat mature landfill leachate, J. Hazard. Mater., 284 (2015) 83–91.
[32] D. Fatta, A. Papadopoulos, M. Loizidou, A study on the landfill leachate and its impact on the groundwater quality of the greater area, Environ. Geochem. Health, 21 (1999) 175–190.
[33] M.A. Zazouli, S. Nasseri, A.H. Mahvi, A.R. Mesdaghinia, M. Gholami, Study of natural organic matter fractions in water sources of Tehran, Pak. J. Biol. Sci., 10 (2007) 1718–1722.
[34] M. Khajeh, Application of Box–Behnken design in the optimization of a magnetic nanoparticle procedure for zinc determination in analytical samples by inductively coupled plasma optical emission spectrometry, J. Hazard. Mater., 172 (2009) 385–389.
[35] B. Kayan, B. Gözmen, Degradation of acid red 274 using H_2O_2 in subcritical water: application of response surface methodology, J. Hazard. Mater., 201 (2012) 100–106.
[36] M.J. Bashir, H.A. Aziz, M.S. Yusoff, New sequential treatment for mature landfill leachate by cationic/anionic and anionic/cationic processes: optimization and comparative study, J. Hazard. Mater., 186 (2011) 92–102.
[37] R.B. D'agostino, A. Belanger, R.B. D'agostino Jr, A suggestion for using powerful and informative tests of normality, Am. Stat., 44 (1990) 316–321.
[38] M. Kuhn, Desirability: Function Optimization and Ranking via Desirability Functions, R package v.2.1, 2016, Available at: https://cran.r-project.org/web/packages/desirability/index.html
[39] P. Kirmizakis, C. Tsamoutsoglou, B. Kayan, D. Kalderis, Subcritical water treatment of landfill leachate: application of response surface methodology, J. Environ. Manage., 146 (2014) 9–15.
[40] Z.M. Abou-Gamra, Kinetic and thermodynamic studies for oxidation of rosaniline hydrochloride dye by persulfate in ambient temperatures, Desal. Water Treat., 57 (2016) 8809–8814.